

Article

In Vivo Nonlinear Optical Imaging of Immune Responses: Tissue Injury and Infection

Yan Zeng,¹ Bo Yan,² Jin Xu,² Qiqi Sun,¹ Sicong He,¹ Jun Jiang,¹ Zilong Wen,^{2,3,*} and Jianan Y. Qu^{1,3,*}¹Biophotonics Research Laboratory, Department of Electronic and Computer Engineering, ²State Key Laboratory of Molecular Neuroscience, Division of Life Science, and ³Center of Systems Biology and Human Health, School of Science and Institute for Advanced Study, Hong Kong University of Science and Technology, Clear Water Bay, Kowloon, Hong Kong SAR, P.R. China

ABSTRACT In this study, we demonstrate a noninvasive imaging approach based on multimodal nonlinear optical microscopy to in vivo image the responses of immune cells (neutrophils) to the tissue injury and bacterial infection in a zebrafish model. Specifically, the second harmonic generation from myosin thick filaments in sarcomere enabled a clear visualization of the muscle injury and infection. Two-photon excited fluorescence was used to track the behavior of the neutrophils that were transgenically labeled by red fluorescent protein. The corresponding reduced nicotinamide adenine dinucleotide (NADH) two-photon excited fluorescence images revealed a detailed morphological transformation process of individual neutrophils during muscle tissue injury and bacterial infection. The analysis of time-resolved NADH signals from the neutrophils provided important biological insights of the cellular energy metabolism during the immune responses. We found a significant increase of free/protein-bound NADH ratios in activated neutrophils in bacterial-infected tissue. In this study, we also discovered that, under 720 nm excitation, two wild-type strains (DH5 α and BL21) of bacteria *Escherichia coli* emitted distinct endogenous fluorescence of double-peak at ~450 and ~520 nm, respectively. We demonstrated that the double-peak fluorescence signal could be used to differentiate the *E. coli* from surrounding tissues of dominant NADH signals, and to achieve label-free tracking of *E. coli* bacteria in vivo.

INTRODUCTION

The response of innate immunity is triggered by the noxious stimulations and conditions, such as infection and tissue injury. The development of immune response implicates the pathogenesis of a large variety of diseases and disorders, including cancer, atherosclerosis, stroke, rheumatoid arthritis, etc. (1,2). This has led to the considerations in understanding the cellular and molecular interactions that are involved in the immune response (1–3). Visualization of the immune response has been achieved by traditional medical imaging methodologies, such as positron emission tomography, computer tomography, magnetic resonance imaging, single-photon emission computed tomography, planar scintigraphy, etc. (4,5). However, these technologies still have many shortcomings, including lacking of adequate resolution for microscopic imaging of individual immune cells, creating unexpected radiological risk to targets and many of them using external contrast agents to enhance image contrast.

To dynamically resolve the motility and migratory behavior of individual immune cells in tissue, confocal microscopy instruments have been combined with new surgical approaches and techniques for imaging cells with

fluorescent labels in tissue, but limited depth of penetration in scattering tissues impedes their further applications (6). In recent years, nonlinear optical microscopy has rapidly evolved as a unique imaging technology to noninvasively record the dynamic nature of fluorescent-labeled immune cells in vivo in deep tissue with fast acquisition of multidimensional imaging (6,7). In addition to tracking of immune cells, quantitative analysis of their functionality becomes an interesting and important research topic. Due to the development of novel photoactivatable fluorescent proteins (8), genetically encoded Förster resonant energy transfer-biosensors (9), and sophisticated optical methodologies including fluorescence recovery after photobleaching and fluorescence correlation spectroscopy (10), the study of immune cell functionality at molecular level now becomes feasible. Moreover, endogenous fluorophores, such as reduced nicotinamide adenine dinucleotide (NADH), are well-known biomarkers of cellular energy metabolism (11). In particular, under ultraviolet (~365 nm for single-photon excitation) or ultrafast near-infrared excitation (~720 nm for two-photon excitation), the endogenous fluorescence of cells is mainly contributed from NAD(P)H (12,13). The two-photon excited NADH fluorescence has been well characterized and applied in many biological studies (14,15). Recently, it has been reported that the spectral and time-resolved fluorescence of NADH, an intrinsic biomarker of energy metabolism, can provide both

Submitted May 28, 2014, and accepted for publication September 9, 2014.

*Correspondence: eequ@ust.hk or zilong@ust.hk

Yan Zeng and Bo Yan contributed equally to this work.

Editor: Mark Cannell.

© 2014 by the Biophysical Society
0006-3495/14/11/2436/8 \$2.00

<http://dx.doi.org/10.1016/j.bpj.2014.09.041>



morphological and functional information for monitoring immune response of bacterial infection of neutrophils in vitro (16). This offers new, to our knowledge, opportunities to study functional activities of immune cells in vivo.

In this study, the endogenous NADH two-photon excited fluorescence (TPEF) is used to noninvasively investigate the cellular energy metabolism of neutrophil in vivo, one type of the important immune cells playing a key role in the defense against invading pathogens. We use zebrafish embryo as the animal model due to its high degree of genetic conservation to human, rapid development, optical transparent, etc. (17). In details, the NADH signals are first extracted from the TPEF image pixels of neutrophil cells that are transgenically labeled by red fluorescence protein (DsRed). We analyze the fluorescence decays of NADH signals and study the cellular metabolism of neutrophils in the typical innate immune response: tissue injury and bacterial infection (3). The injury induced by a single acupuncture of glass needle and bacterial infection caused by bacterial injection are manually created in the skeletal muscle of zebrafish. The trauma caused by the mechanical injury can be clearly visualized by the alterations of cellular profile in the muscle formed with NADH signals. Muscle cell damage is also identified by morphological changes of myosin thick filaments in sarcomere that can be efficiently probed by second harmonic generation (SHG) signals as well (18). To further study the energy metabolism of neutrophils, we analyze the temporal characteristics of NADH fluorescence. Additionally, we demonstrate the distinct endogenous TPEF signals from two wild-type (WT) strains of commonly used bacterial model *Escherichia coli* can be used for label-free in vivo tracking bacterial.

MATERIALS AND METHODS

TPEF and SHG imaging system

The combined TPEF and SHG imaging microscope was modified from our previous system (16). The schematic diagram of the system is described in Fig. 1. The excitation source was from a standard femtosecond Ti/sapphire laser (Mira 900, Coherent) tuned at 720 nm. The excitation light was then expanded, collimated, and directed to a water immersion objective lens (UAPON 40XW340, 1.15 NA, Olympus) which was used to focus the excitation beam onto the samples and collect backscattered TPEF. To avoid any tissue damage and photobleaching, the excitation power was kept below 15 mW at the back aperture of the objective. The TPEF emission from the sample was reflected by a dichroic mirror (T600LPXR, Chroma) and relayed by a telescope to the detection system. In the experiment of visualizing immune response, the TPEF signals with wavelength shorter than 475 nm (dominant by NADH signals) was reflected to a single-channel hybrid detector equipped with a time-correlated single photon counting (TCSPC) module (HPM-100-40, SPC150, Becker & Hickl) by a movable dichroic mirror (475DCRXU, Chroma). A bandpass filter: 440 ± 40 nm (Chroma) was used to further purify the NADH signals. The fluorescence signals with wavelength longer than 475 nm were directed to a circle-to-line fiber bundle, which guided the light to a spectrograph (Ocean Optics) equipped with a 16 photomultiplier array (PML-16-C-0 and SPC-150, Becker & Hickl). The TPEF signals recorded in time and spectral domain from 475 to 600 nm were green fluorescent protein (GFP) and DsRed.

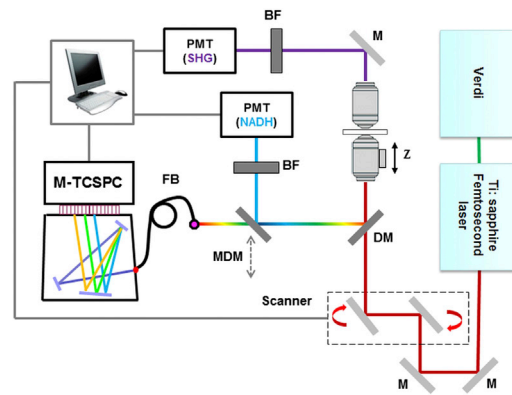


FIGURE 1 Schematic diagram of the TPEF and SHG imaging system. PMT: photomultiplier tube; BF: bandpass filter; BS: beam splitter; M: mirror; DM: dichroic mirror; MDM: movable dichroic mirror; FB: fiber bundle; M-TCSPC: time-correlated single photon counting (TCSPC) module equipped with a multichannel PMT array. To see this figure in color, go online.

In the experiment of label-free in vivo tracking bacteria using the distinct double-peak of TPEF signals from wild strain *E. coli*, the dichroic mirror was removed and all the emitted backscattered fluorescence from 400 to 600 nm was directed to a fiber bundle for spectral-resolved detection. To record the SHG image, the forward SHG signals were collected by a water immersion objective (LUMPLFLN 40XW, 0.8 NA, Olympus), purified by a bandpass filter (FF01-357/44, Semrock), and guided to a cooled photomultiplier tube (PMC-100-4 and SPC-150, Becker & Hickl). Regular TPEF and SHG images of $90 \times 90 \mu\text{m}^2$, corresponding to 256×256 pixels, were created by scanning a pair of galvo mirrors. The imaging depth was controlled by an actuator. The interval for depth-resolved imaging was 1 μm . The zebrafish embryo was sandwiched by two coverslips with $\sim 400 \mu\text{m}$ gap and monitored by brightfield imaging with illumination of a white light source before imaging. To clearly display the TPEF and SHG images, the TPEF images of DsRed, GFP, and NADH were coded in red, green, and yellow, respectively, whereas the SHG image was coded in cyan. To directly measure the time course of the NADH fluorescence decay, an image-guided method was applied to collect the NADH signals from the pixels of neutrophils for time-resolved analysis using a dual exponential decay model: $A_1 \cdot \exp(-t/\tau_1) + A_2 \cdot \exp(-t/\tau_2)$ (16,19). Here, τ_1 and τ_2 indicate a short fluorescence lifetime component for free NADH and long-lifetime component for protein-bound NADH, respectively. Two lifetime components A_1 and A_2 represent the relative contribution of the free NADH and protein-bound NADH, respectively. The detecting range of fluorescence lifetime is 12.5 ns, which is determined by the repetition rate of the laser (80 MHz). In this study, the student's *t*-test is used to compare the quantitative results.

Animal model and bacterial preparation

The zebrafish WT strain AB and transgenic *Tg(lyz:DsRed2)nz50* were raised up under standard condition (20,21). Embryos were maintained in egg water containing 0.2 mM *N*-phenylthiourea (PTU) (Sigma) to prevent pigment formation (21). For imaging, 2 days postfertilization (dpf) embryos were mounted in 1.2% low melting agarose on glass slides with 0.02% tricaine for anesthesia before the application of injury or infection treatment (22). Injury was induced via a single acupuncture with a glass needle (16 μm diameter) in the skeletal muscle of 2 dpf *Tg(lyz:DsRed2)nz50* embryos. Infection was performed by injecting bacteria into the skeletal muscle of 2 dpf *Tg(lyz:DsRed2)nz50* embryos via the glass needle. Bacteria DH5 α , DH10B, BL21, ORN178, and DH5 α (containing pDSK-GFP) were cultured in liquid lysogeny broth media at 37°C for ~ 16 h with

vigorous shaking (~300 rpm), and were harvested by centrifugation at $5000 \times g$ for 5 min and resuspended in sterile phosphate buffered saline (23). In vivo microscopic imaging was conducted ~2 h after tissue injury or bacterial injection. For antiinflammation drug treatment, embryos were preincubated with PTU egg water containing $800 \mu\text{M}$ dexamethasone for ~12 h before the injury and infection (22).

RESULTS AND DISCUSSION

NADH TPEF and myosin SHG imaging reveal tissue structures in zebrafish

Skeletal muscle, composing up to 45% of the total body mass, is the most abundant tissue in the human body (24). Diagnosis of acute muscle injury and inflammatory myopathies requires histological assessment to investigate muscle inflammation. In addition, scientific literature for decades indicates that immune cells such as neutrophils and macrophages play regulatory roles in muscle development, repair, and regeneration (25). Therefore, it is meaningful and valuable to study inflammation in vivo by using skeletal muscle. Before inflammatory treatment, we first imaged the normal skeletal muscle in zebrafish embryo (*Tg(lyz:DsRed2)nz50*).

Fig. 2, A–C, show the typical TPEF and SHG images taken in the skeletal muscle layer above the dorsal vein and aorta. Without inflammation, rare immune cells such as neutrophils stay in the muscle layer, shown by the TPEF image formed with DsRed signals in Fig. 2 A. The corresponding TPEF image of NADH (Fig. 2 B) gives the morphology of tubular structure of mitochondria in the pixels with higher fluorescence intensity compared to that in the cytosol (26). The SHG signals in Fig. 2 C also reveal the compact structure of these muscle cells and indicate the location of the periodic myosin thick filaments. The bright tubular mitochondria located between the muscle fibers are shown in the merged image (Fig. 2 D) of the DsRed, NADH TPEF image, and SHG image of myosin thick filaments. The long, cylindrical and multinucleated features of myofibers are clearly visualized. Below the skeletal muscle layer, many resting neutrophils marked by the DsRed signals (figured out by the circles in Fig. 2 E) were found

in the blood islands located between the vein and aorta that are considered as the intermediate hematopoietic organ in the early development of the zebrafish (27). Specifically, round shape and multilobe nucleus structure of neutrophil can be clearly identified in the NADH TPEF image of the in-focus neutrophil marked with the white circle in Fig. 2, F and H. During innate immune response, these neutrophils are reported to be quickly activated and migrate to the inflammatory site within a few hours (28). In addition, the region with vertical dark lines marked by red arrows in Fig. 2, F and H, was the blood vessel filled with flowing red blood cells, where the plasma TPEF signal produced negative contrast for the images of red blood cells and the dark lines were distorted images of flowing red blood cells (29).

Characterization of tissue injury in skeletal muscle

The injury in the skeletal muscle layer of zebrafish embryos was created by a single acupuncture with a glass needle ($16 \mu\text{m}$ in diameter). These zebrafish embryos with injury and the control group were then examined by our home-built microscope system. Fig. 3, A–C, show the representative TPEF and SHG images, taken in the wounds of skeletal muscle. The image formed with DsRed signals in Fig. 3 A clearly identifies the neutrophils of ruffle shape. The corresponding NADH TPEF image (Fig. 3 B) displays the morphological structure of the neutrophil with bright NADH signals in the cytosol and weak NADH signals in the nucleus (16). In addition, distorted tissue structure (a dark hole in Fig. 3 B) in the wounded region shows the damage of the compact and regulated muscle cells. This is more clearly shown in the corresponding SHG image in Fig. 3 C and merged image in Fig. 3 D. The large dark hole without any SHG signals represents the regions without muscle cells or with damaged muscle structure. This was caused by mechanical damage of muscle cells and tissue.

Next, to study the energy metabolism of activated neutrophils, we extract the NADH signals from the pixels of neutrophil marked by the guiding star of DsRed signals in

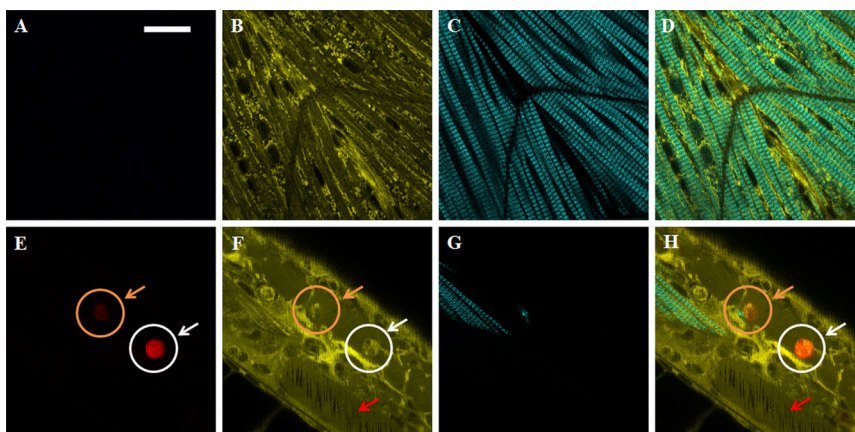


FIGURE 2 TPEF and SHG images of skeletal muscle in control zebrafish embryo. (A–C) TPEF and SHG images of skeletal muscle layer (images were formed with DsRed, NADH, and SHG signals, respectively); (D) merged image of (A–C); (E–G) TPEF and SHG images of resting neutrophils in the tissue near vasculature (images were formed with DsRed, NADH, and SHG signals, respectively); (H) merged image of (E–G); Orange and white circle pointing out the DsRed labeled neutrophils in out-of-focus and in-focus locations, respectively; Red arrow pointing out the dorsal aorta; Scale bar $20 \mu\text{m}$. To see this figure in color, go online.

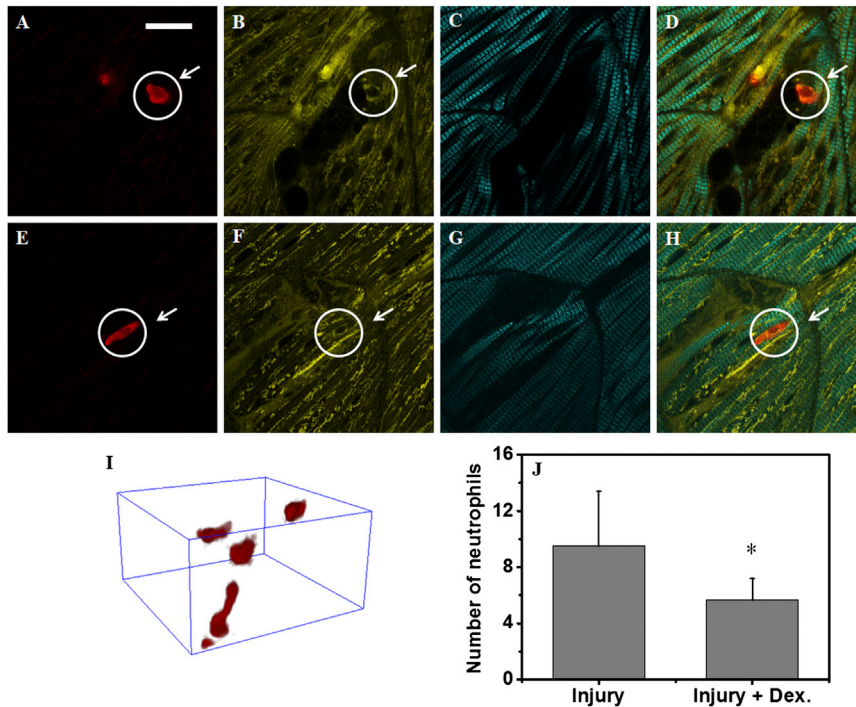


FIGURE 3 TPEF and SHG images of skeletal muscle with tissue injury. (A–C) TPEF and SHG images of injured skeletal muscle (images were formed with DsRed, NADH, and SHG signals, respectively); (D) merged image of (A–C); (E–G) TPEF and SHG images of injured skeletal muscle from zebrafish embryo treated with Dexamethasone (images were formed with DsRed, NADH, and SHG signals, respectively); (H) merged image of (E–G); (I) 3D reconstruction of DsRed-labeled neutrophils in the wounds; (J) quantitative counting of neutrophils accumulated in the wounds (the values are based on the measurements of 10 zebrafish embryos). Image size: $90 \times 90 \mu\text{m}^2$ (256×256 pixels); *indicating p value < 0.01; Scale bar: $20 \mu\text{m}$. To see this figure in color, go online.

each TPEF image for fluorescence lifetime analysis (19). Because the fluorescent peak of DsRed (~ 585 nm) is far away from the fluorescence peak of NADH (~ 450 nm), there was no interference to the NADH channel from the DsRed fluorescence (16). The extracted NADH signals mainly come from cytosol due to the facts: 1), the cellular energy metabolism of neutrophil is dominated by the glycolysis pathway in cytosol and the presence of mitochondria in the cell body of neutrophil is rare (30); 2), NADH signals from nucleus are much weaker than that in the cytosol and negligible (shown in Fig. 3, B and F). The NADH fluorescence decays were analyzed by using a dual exponential function model (19). The results are summarized in Table 1. As can be seen, in both the control zebrafish embryos and the fish with tissue injury, the short fluorescence lifetime component (τ_1) of NADH fluorescence decays is kept around ~ 0.4 ns, which is reported to be generated from free NADH (19). The long-lifetime component (τ_2) is attributed to the protein-bound NADH. It has been reported that the fluorescence lifetime of NADH changes depending on the protein or enzyme that NADH is bound to (31). Therefore, the variation of the long-lifetime component τ_2 as shown in Table 1 could be caused by the changes of the enzyme binding sites for NADH under different conditions. Furthermore, the dependence of NADH lifetime on its bound protein also provides a possible explanation why we observed a larger long fluorescence lifetime component ($\tau_2 \sim 8.0$ ns) in the tissue of zebrafish compared to the cultured cells or tissues in other animals of different species (13,19,32). However, the exact reason that τ_2 in zebrafish is much longer still remains unknown. The increase of free

over protein-bound NADH ratio (A_1/A_2) indicates that the energy consumed in the activated neutrophils is mainly produced through the glycolysis pathway, leading to the accumulation of free NADH (16,30).

It is known that severe inflammation could result in tissue damage and disorder, leading to functional loss of our body organs (1–3). The standard treatment is the administration of effective antiinflammatory medications (33). Therefore, it is interesting and important to study the functional behavior of immune cells with antiinflammation treatment. We analyzed the NADH signals of the neutrophils in the injured tissue after the zebrafish embryo was treated with a widely used antiinflammation steroid drug, Dexamethasone (33). Fig. 3, E–H, show the typical TPEF and SHG images, taken in the wounds of skeletal muscle in treated zebrafish embryo. To have a quantitative evaluation of the antiinflammatory treatment, we reconstruct the three-dimensional (3D) distribution of neutrophils in the wounds

TABLE 1 A_1/A_2 ratio and lifetimes measured from neutrophil^{a,b}

	τ_1 (ns)	τ_2 (ns)	A_1/A_2
Control	0.37 ± 0.02	8.3 ± 1.1	2.98 ± 0.27
Injury	0.39 ± 0.03	$6.7 \pm 1.0^*$	$3.35 \pm 0.23^*$
Infection	0.34 ± 0.01	$7.3 \pm 1.0^*$	$3.93 \pm 0.32^*$
Control + Dex.	0.37 ± 0.02	8.8 ± 1.1	3.01 ± 0.34
Injury + Dex.	0.36 ± 0.02	$5.5 \pm 0.7^*$	$4.27 \pm 0.71^*$
Infection + Dex.	0.36 ± 0.02	$6.7 \pm 1.0^*$	$4.05 \pm 0.39^*$

^aRatios and lifetimes are calculated with the NADH fluorescence decays.

^bThe values of all parameters are based on the average over >20 TPEF images from 10 zebrafish embryos; *indicating p value < 0.01.

by using a stack of depth-resolved DsRed TPEF images with a $0.5\ \mu\text{m}$ depth-sectioning interval. A representative reconstructed 3D image of neutrophils in the volume of injured tissue is shown Fig. 3 I. As can be seen, individual neutrophils in the imaging volume throughout the injury site can be clearly counted. The statistical results of neutrophil counting are shown in Fig. 3 J. A significant decrease of neutrophils was observed, indicating the antiinflammation effect of Dexamethasone (33). The time-resolved analysis of NADH fluorescence signals for control and Dexamethasone-treated zebrafish embryos are summarized in Table 1. For the control group, we found that Dexamethasone did not alter the metabolic status of resting neutrophils because the fluorescence lifetime components and A_1/A_2 -ratio were almost unchanged. However, for the zebrafish embryos with tissue injury, free over protein-bound NADH ratio in the neutrophil cells increased significantly after the treatment of Dexamethasone, consistent with the fact that Dexamethasone reduced the production of radical oxygen species (34,35), leading to decreased consumption of NADPH, which is the phosphate form of NAD and has similar fluorescence characteristics to NADH. The results demonstrate that the time-resolved NADH fluorescence can be potentially used for label-free monitoring of metabolic dynamics of immune cells in the inflammation induced by tissue injury.

Immune response of neutrophil against bacterial infection

Bacterial infection remains one of the major challenges to human society. It is known that the invasion of a host organism's bodily tissues by disease-causing pathogens will lead to serious inflammatory response (3,36). To study the immune response of neutrophil against bacterial infection, GFP-labeled bacteria *E. coli* was injected into the skeletal muscle layer of zebrafish embryo. Fig. 4, A–C, show the typical TPEF and SHG images recorded in the area of bacterial injection. The TPEF image of DsRed (Fig. 4 A) clearly

shows the morphological feature of activated neutrophils, which migrated to phagocytose the *E. coli*. In particular, the neutrophils in Fig. 4 A are turned to ruffle shapes. Individual circular phagosomes with much less DsRed signals are visualized inside the neutrophils' bodies (pointed out by the white arrows in Fig. 4 A).

To further study the phagocytosis process, we formed a combined TPEF image with the signals from NADH (collected by a hybrid photomultiplier tube (PMT)) and GFP signal band (488 to 527 nm), shown in Fig. 4 B. The pixels coded in green, dominated by GFP signals, indicate the locations of *E. coli*, which is consistent with the location of phagosomes, where the neutrophils engulf and kill bacteria. The round shape morphology of the *E. coli*, shown in Fig. 4 B may be due to the facts that the phagosomes simultaneously phagocytosed several *E. coli*, or the damage of bacterial cell membrane could cause the diffusive GFP into the phagosome. It should be emphasized that the TPEF image formed with GFP signal band alone does not provide sufficient differentiation of *E. coli* from the surrounding tissue because the GFP signals are interfered by the tail of NADH signals under 720 nm excitation, the inefficient excitation wavelength for GFP (37). Therefore, the usage of the TPEF image formed by the signals from the pure NADH channel (the hybrid PMT) as a reference in the combined TPEF image (Fig. 4 B) is critical to eliminate the interference of NADH signals and enhance the contrast of GFP-labeled bacteria. The SHG image in Fig. 4 C indicates the injury site and the merged image Fig. 4 D provides rich information to visualize the function of the immune cells in the skeletal muscle. The 3D reconstruction of neutrophils in the infectious tissue volume in Fig. 4 E shows the accumulation of a much larger number of neutrophils in comparison with the tissue injury. The results are quantitatively verified in the counting of neutrophils as displayed in Fig. 4 F. The time-resolved analyses of NADH fluorescence from activated neutrophils are summarized in Table 1. The results show that a significantly higher free over

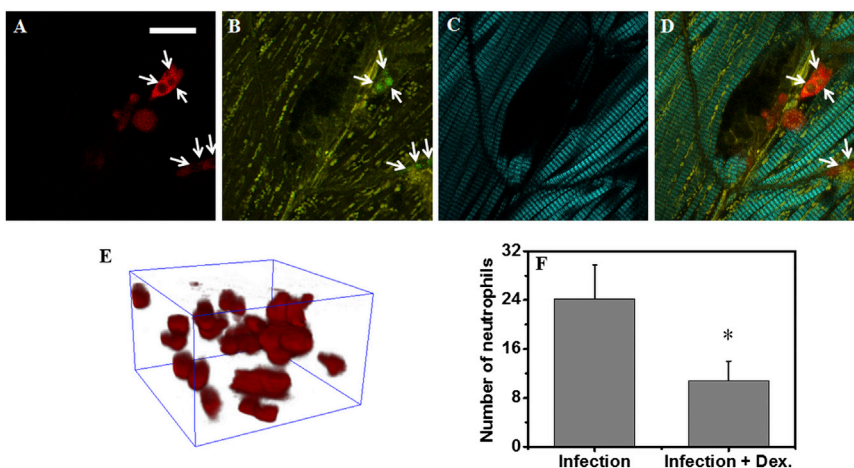


FIGURE 4 TPEF and SHG images of skeletal muscle with bacterial infection. (A) TPEF image of neutrophils, formed with DsRed signals; (B) combined TPEF image, formed with NADH and GFP signals (white arrows indicate GFP-labeled *E. coli*); (C) SHG images of skeletal muscle layer; (D) merged image with the signals from DsRed, NADH, and SHG; (E) 3D reconstruction of DsRed-labeled neutrophils; (F) quantitative counting of neutrophils accumulated in the wound (the values are based on the measurements of 10 zebrafish embryos). Image size: $90 \times 90\ \mu\text{m}^2$ (256×256 pixels); *indicating p value < 0.01 ; Scale bar: $20\ \mu\text{m}$. To see this figure in color, go online.

protein-bound NADH (A_1/A_2) ratio up to ~ 4.0 , indicating a higher demand of energy metabolism in neutrophils against bacterial infection than in tissue injury. In the study of anti-inflammation treatment with Dexamethasone, we found that the treatment reduces the number of accumulated neutrophils as shown Fig. 4 F, whereas the high activation of energy metabolism is maintained because the A_1/A_2 -ratio remained almost unchanged as displayed in Table 1.

Label-free tracking bacteria *E. coli*

Dynamic tracking of bacteria is essential for understanding bacterial invasion and infection, tissue resolution, and antimicrobial treatment (38,39). Though we used fluorescence protein-labeled *E. coli* to track the bacteria and study the phagocytosis of neutrophils, it is desirable to image the bacteria based on their intrinsic fluorescence because the fluorescence proteins can be reserved to label other important immune cells and tissue structures, such as macrophages and endothelium of blood vessel. In this study, we discovered that two WT strains of *E. coli* emit distinct endogenous fluorescence with double-peak spectral structure under near-infrared excitation at 720 nm. The double-peak spectral lineshape provide contrast to the tissue fluorescence dominated by NADH signals in many animal models such as zebrafish, mice, etc. (28,40). This distinct fluorescence signal can be used for label-free in vivo tracking of bacteria and their activities.

To study the spectral characteristics of bacteria *E. coli*, we first remove the dichroic mirror in the backward detection system to allow all the backscattered fluorescence signals entering into the fiber bundle for spectral resolved imaging.

Fig. 5 A shows a typical TPEF fluorescence image of WT *E. coli* strain (DH5 α) where rod-shaped cell bodies can be identified. The fluorescence spectra of several WT strains of *E. coli* (DH5 α , DH10B, BL21, and ORN178) are display in Fig. 5 B. The result shows that two WT strains DH5 α and DH10B emit distinct double-peak spectral lineshape. The fluorescence peaked at ~ 450 nm is dominated by NADH under 720 nm excitation, whereas the fluorescence peaked at ~ 520 nm may be generated by other endogenous fluorophore such as flavin adenine dinucleotide (FAD) because FAD was reported to be overproduced by some specific strains of bacteria *E. coli* during exponential growth (41). To further study the characteristics of endogenous fluorescence, we measured the TPEF signals of WT strain DH5 α under different excitation wavelength (Fig. 5 C). With longer wavelength excitation, the NADH dominant peak was significantly reduced and a single fluorescence peak at 520 nm remained unchanged. This is consistent with the excitation of FAD fluorescence (42). Next, we analyzed the fluorescence lifetime decay of the fluorescence signal recorded at 520 nm channel and found two fluorescence lifetime components ~ 2.93 and ~ 0.23 ns that are consistent with the fluorescence lifetime of free FAD and protein-bound FAD, respectively (42). Furthermore, we manipulated the cellular metabolism of bacteria by treating the cells with mitochondrial inhibitor sodium cyanide (NaCN) and uncoupler carbonyl cyanide 3-chlorophenylhydrazone (CCCP). Fig. 5 D shows the results of fluorescence spectral of *E. coli* (WT strain DH5 α) under treatment of metabolic stress. The effects of NaCN and CCCP on the signals at the NADH peak at 450 nm and FAD peak at 520 nm are consistent with previous study (19,42,43). All the results

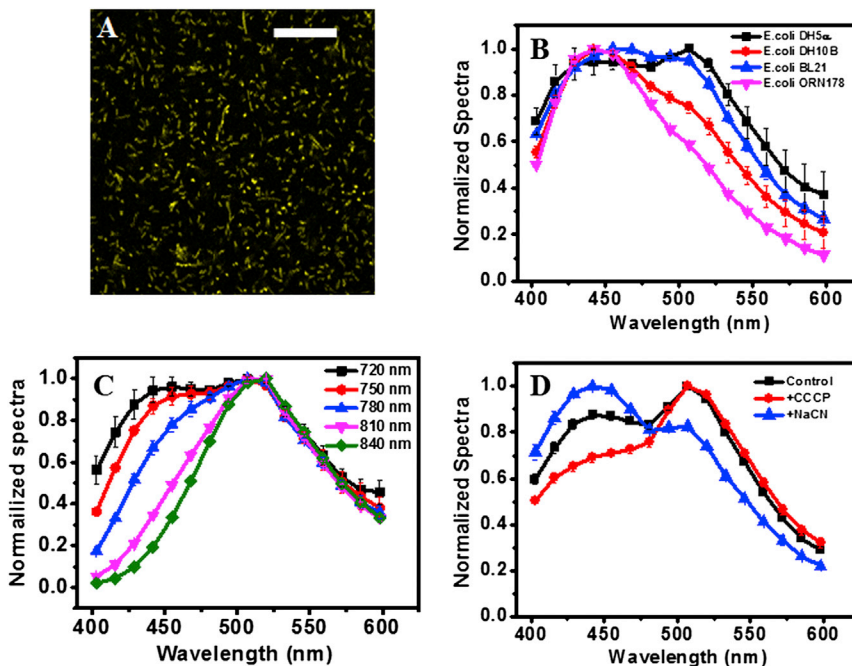


FIGURE 5 Fluorescence characteristics of bacterial cells. (A) TPEF images of *E. coli* (DH5 α); (B) normalized fluorescence spectral of different strains of *E. coli* (DH5 α , DH10B, BL21, and ORN178) under 720 nm excitation; (C) normalized fluorescence spectra of TPEF images of *E. coli* (DH5 α) under 720 nm, 750 nm, 780 nm, 810 nm, and 840 nm excitation, respectively; (D) normalized fluorescence spectra of *E. coli* (DH5 α) under different metabolic stimulation: CCCP, and NaCN, excited at 720 nm. The acquisition time for the TPEF image: 32 s; Resolution: 256×256 pixels for $90 \times 90 \mu\text{m}^2$; Scale bar $20 \mu\text{m}$. To see this figure in color, go online.

indicate that the fluorescence peaked at 520 nm is likely to be generated by FAD.

To demonstrate the distinct double-peak fluorescence can be used for label-free *in vivo* tracking bacteria, the *E. coli* (WT strain DH5 α) was injected into the skeletal muscle of zebrafish embryo (strain AB). Fig. 6 A display a representative TPEF image captured in the infectious region. The NADH fluorescence dominant band of 403–481 nm was coded in yellow, whereas the signals from 495 to 598 nm were coded in cyan. In Fig. 6 A, individual circular phagosome containing *E. coli* can be clearly identified (marked out by the white arrows). The extracted fluorescence spectra of muscle tissue and *E. coli* are shown in Fig. 6 B. It can be seen that the distinct double-peak spectral lineshape remains unchanged when the bacteria is injected into live zebrafish, providing the fundamental evidence that the contrast between bacteria and tissue are indeed from the distinct endogenous fluorescence of *E. coli* (WT strain DH5 α). This was further verified by the fact that phagosome does not emit autofluorescence under ultrafast near-infrared excitation (20). It should be emphasized that this label-free imaging method based on specific double-peak fluorescence spectrum of *E. coli* can provide good imaging contrast in the biological tissue because most of the intrinsic/extrinsic fluorophores only emit single-peak fluorescence spectrum dominated by the NADH signal.

CONCLUSION

In this study, we demonstrated the multimodal nonlinear optical imaging as a promising tool to study the functional behavior of immune cell (neutrophil) in inflammatory processes of tissue injury and bacterial infection. The two-photon excitation NADH fluorescence provided biochemical information for monitoring energy metabolism during neutrophil activation, whereas SHG signals gave complementary image to identify the tissue damage. This method-

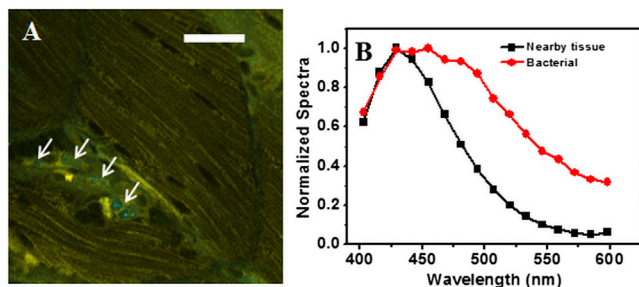


FIGURE 6 Label-free imaging bacteria in live animal *in vivo*. (A) TPEF image of infectious muscle tissue of zebrafish; (B) normalized fluorescence spectra of bacterial cells and muscle tissue. The acquisition time for each TPEF image: 32 s; Size of each TPEF image: $90 \times 90 \mu\text{m}^2$. The signals from the wavelength range of 403–481 nm are coded in green color and the signals from the wavelength range of 495–598 nm are coded in cyan. The white arrows point out the positions of the bacterial cells in the TPEF images; Scale bar $20 \mu\text{m}$. To see this figure in color, go online.

ology can be further extended to study functional activities of other immune cells such as macrophage or lymphocyte in future study. We also demonstrated that the animal model and imaging technique can be potentially used to study the effect of new antiinflammatory medications and strategy of antiinflammation treatment. The discovery of distinct double-peak fluorescence spectrum of *E. coli* strain DH5 α and BL21 enable new opportunities, to our knowledge, to label-free *in vivo* track bacteria in animal model.

This work was supported by the Hong Kong Research Grants Council through grants 662711, N_HKUST631/11, T13-607/12R and T13-706/11-1, AOE/M-09/12, and HKUST through grant RPC10EG33.

REFERENCES

- Pier, G. B., J. B. Lyczak, and L. M. Wetzler. 2004. Immunology, Infection, and Immunity. ASM Press, Washington, DC.
- Kumar, V., R. S. Cotran, and S. L. Robbins. 2003. Robbins Basic Pathology. Saunders, Philadelphia, PA.
- Medzhitov, R. 2008. Origin and physiological roles of inflammation. *Nature*. 454:428–435.
- Hildebrandt, I. J., and S. S. Gambhir. 2004. Molecular imaging applications for immunology. *Clin. Immunol.* 111:210–224.
- Gotthardt, M., C. P. Bleeker-Rovers, ..., W. J. G. Oyen. 2010. Imaging of inflammation by PET, conventional scintigraphy, and other imaging techniques. *J. Nucl. Med.* 51:1937–1949.
- Germain, R. N., M. J. Miller, ..., M. C. Nussenzweig. 2006. Dynamic imaging of the immune system: progress, pitfalls and promise. *Nat. Rev. Immunol.* 6:497–507.
- Yamanaka, Y. J., T. M. Gierahn, and J. C. Love. 2013. The dynamic lives of T cells: new approaches and themes. *Trends Immunol.* 34:59–66.
- Victoria, G. D., T. A. Schwickert, ..., M. C. Nussenzweig. 2010. Germinal center dynamics revealed by multiphoton microscopy with a photoactivatable fluorescent reporter. *Cell*. 143:592–605.
- Paster, W., C. Paar, ..., H. Stockinger. 2009. Genetically encoded Förster resonance energy transfer sensors for the conformation of the Src family kinase Lck. *J. Immunol.* 182:2160–2167.
- Lippincott-Schwartz, J., E. Snapp, and A. Kenworthy. 2001. Studying protein dynamics in living cells. *Nat. Rev. Mol. Cell Biol.* 2:444–456.
- Monici, M. 2005. Cell and tissue autofluorescence research and diagnostic applications. *Biotechnol. Annu. Rev.* 11:227–256.
- Salmon, J. M., E. Kohen, ..., B. Thorell. 1982. Microspectrofluorometric approach to the study of free/bound NAD(P)H ratio as metabolic indicator in various cell types. *Photochem. Photobiol.* 36:585–593.
- Huang, S., A. A. Heikal, and W. W. Webb. 2002. Two-photon fluorescence spectroscopy and microscopy of NAD(P)H and flavoprotein. *Biophys. J.* 82:2811–2825.
- Balaban, R. S., and L. J. Mandel. 1990. Optical methods for the study of metabolism in intact cells. In *Noninvasive Techniques in Cell Biology*. J. K. Foskett and S. Grinstein, editors. Wiley-Liss, New York, pp. 213–236.
- Lakowicz, J. R. 2006. Principles of Fluorescence Spectroscopy. Springer, New York.
- Zeng, Y., B. Yan, ..., J. Y. Qu. 2013. Label-free *in vivo* imaging of human leukocytes using two-photon excited endogenous fluorescence. *J. Biomed. Opt.* 18:040504.
- Kar, B., and S. Subbiah. 2013. Zebrafish: an *in vivo* model for the study of human diseases. *Inter. J. Genet. & Genomics.* 1:6–11.
- Nucciotti, V., C. Stringari, ..., F. S. Pavone. 2010. Probing myosin structural conformation *in vivo* by second-harmonic generation microscopy. *Proc. Natl. Acad. Sci. USA.* 107:7763–7768.

19. Li, D., W. Zheng, and J. Y. Qu. 2008. Time-resolved spectroscopic imaging reveals the fundamentals of cellular NADH fluorescence. *Opt. Lett.* 33:2365–2367.
20. Hall, C., M. V. Flores, ..., P. Crosier. 2007. The zebrafish lysozyme C promoter drives myeloid-specific expression in transgenic fish. *BMC Dev. Biol.* 7:42.
21. Westerfield, M. 1995. *The Zebrafish Book: A Guide for the Laboratory Use of Zebrafish (Danio rerio)*. Eugene, OR.
22. Yan, B., P. Han, ..., Z. Wen. 2014. IL-1 β and reactive oxygen species differentially regulate neutrophil directional migration and Basal random motility in a zebrafish injury-induced inflammation model. *J. Immunol.* 192:5998–6008.
23. Benard, E. L., A. M. van der Sar, ..., A. H. Meijer. 2012. Infection of zebrafish embryos with intracellular bacterial pathogens. *J. Vis. Exp.* 61:e3781.
24. Janssen, I., S. B. Heymsfield, ..., R. Ross. 2000. Skeletal muscle mass and distribution in 468 men and women aged 18–88 yr. *J. Appl. Physiol.* 89:81–88.
25. Schiaffino, S., and T. Partridge. 2008. *Skeletal Muscle Repair and Regeneration*. Springer, New York.
26. Sun, Q., Y. Li, ..., J. Y. Qu. 2013. Label-free multimodal nonlinear optical microscopy reveals fundamental insights of skeletal muscle development. *Biomed. Opt. Express.* 5:158–166.
27. Jin, H., J. Xu, and Z. Wen. 2007. Migratory path of definitive hematopoietic stem/progenitor cells during zebrafish development. *Blood.* 109:5208–5214.
28. Li, J. L., and L. G. Ng. 2012. Peeking into the secret life of neutrophils. *Immunol. Res.* 53:168–181.
29. Zeng, Y., B. Yan, ..., J. Y. Qu. 2014. In vivo micro-vascular imaging and flow cytometry in zebrafish using two-photon excited endogenous fluorescence. *Biomed. Opt. Express.* 5:653–663.
30. Kominsky, D. J., E. L. Campbell, and S. P. Colgan. 2010. Metabolic shifts in immunity and inflammation. *J. Immunol.* 184:4062–4068.
31. Iweibo, I. 1976. Protein fluorescence and electronic energy transfer in the determination of molecular dimensions and rotational relaxation times of native and coenzyme-bound horse liver alcohol dehydrogenase. *Biochim. Biophys. Acta.* 446:192–205.
32. Stringari, C., A. Cinquin, ..., E. Gratton. 2011. Phasor approach to fluorescence lifetime microscopy distinguishes different metabolic states of germ cells in a live tissue. *Proc. Natl. Acad. Sci. USA.* 108:13582–13587.
33. d'Alençon, C. A., O. A. Peña, ..., M. L. Allende. 2010. A high-throughput chemically induced inflammation assay in zebrafish. *BMC Biol.* 8:151.
34. Cooper, M. R., L. R. DeChatelet, and C. E. McCall. 1972. The in vitro effect of steroids on polymorphonuclear leukocyte metabolism. *Proc. Soc. Exp. Biol. Med.* 141:986–990.
35. Coates, T. D., B. Wolach, ..., L. A. Boxer. 1983. The mechanism of action of the antiinflammatory agents dexamethasone and Auranofin in human polymorphonuclear leukocytes. *Blood.* 62:1070–1077.
36. Ashley, N. T., Z. M. Weil, and R. J. Nelson. 2012. Inflammation: mechanisms, costs, and natural variation. *Annu. Rev. Ecol. Evol. Syst.* 43:385–406.
37. Drobizhev, M., N. S. Makarov, ..., A. Rebane. 2011. Two-photon absorption properties of fluorescent proteins. *Nat. Methods.* 8:393–399.
38. Cronin, M., A. R. Akin, ..., M. Tangney. 2012. High resolution in vivo bioluminescent imaging for the study of bacterial tumour targeting. *PLoS ONE.* 7:e30940.
39. Leevy, W. M., S. T. Gammon, ..., B. D. Smith. 2006. Optical imaging of bacterial infection in living mice using a fluorescent near-infrared molecular probe. *J. Am. Chem. Soc.* 128:16476–16477.
40. Teh, S. K., W. Zheng, ..., J. Y. Qu. 2013. Multimodal nonlinear optical microscopy improves the accuracy of early diagnosis of squamous intraepithelial neoplasia. *J. Biomed. Opt.* 18:036001.
41. Wilson, A. C., and A. B. Pardee. 1962. Regulation of flavin synthesis by *Escherichia coli*. *J. Gen. Microbiol.* 28:283–303.
42. Wu, Y., and J. Y. Qu. 2006. Combined depth- and time-resolved autofluorescence spectroscopy of epithelial tissue. *Opt. Lett.* 31:1833–1835.
43. Chance, B., B. Schoener, ..., Y. Nakase. 1979. Oxidation-reduction ratio studies of mitochondria in freeze-trapped samples. NADH and flavoprotein fluorescence signals. *J. Biol. Chem.* 254:4764–4771.